

Article

Three-Dimensional Non-Linearly Thermally Radiated Flow of Jeffrey Nanoliquid towards a Stretchy Surface with Convective Boundary and Cattaneo–Christov Flux

Kandasamy Jagan ¹  and Sivanandam Sivasankaran ^{2,*} 

¹ Department of Mathematics, School of Engineering, Presidency University, Bangalore 560064, India

² Mathematical Modelling and Applied Computation Research Group, Department of Mathematics, King Abdulaziz University, Jeddah 21589, Saudi Arabia

* Correspondence: sd.siva@yahoo.com

Abstract: The objective of this paper is to investigate the 3D non-linearly thermally radiated flow of a Jeffrey nanofluid towards a stretchy surface with the Cattaneo–Christov heat flux (CCHF) model in the presence of a convective boundary condition. The Homotopy Analysis Method (HAM) is used to solve the ordinary differential equation that is obtained by reforming the governing equation using suitable transformations. The equations obtained from HAM are plotted graphically for different parameters. In addition, the skin-friction coefficient, local Nusselt number, and Sherwood number for various parameters are calculated and discussed. The velocity profile along the x- and y-directions decrease with a raise in the ratio of relaxation to retardation times. The concentration and temperature profile rises while magnifying the ratio of relaxation to retardation times. While raising the ratio parameter, the x-direction velocity, temperature, and concentration profile diminishes, whereas the y-direction velocity profile magnifies. Magnifying the Deborah number results in a rise in the velocity profile along the x- and y-directions, and a decline in the temperature and concentration profile.

Keywords: 3D flow; Jeffrey nanofluid; stretchy surface; non-linear thermal radiation



Citation: Jagan, K.; Sivasankaran, S. Three-Dimensional Non-Linearly Thermally Radiated Flow of Jeffrey Nanoliquid towards a Stretchy Surface with Convective Boundary and Cattaneo–Christov Flux. *Math. Comput. Appl.* **2022**, *27*, 98. <https://doi.org/10.3390/mca27060098>

Academic Editor: Zhuojia Fu

Received: 15 March 2022

Accepted: 16 November 2022

Published: 19 November 2022

Publisher's Note: MDPI stays neutral with regard to jurisdictional claims in published maps and institutional affiliations.



Copyright: © 2022 by the authors. Licensee MDPI, Basel, Switzerland. This article is an open access article distributed under the terms and conditions of the Creative Commons Attribution (CC BY) license (<https://creativecommons.org/licenses/by/4.0/>).

1. Introduction

There are many models for a non-Newtonian fluid, and a few of them have been discussed in Halim et al. [1], Mahanthesh et al. [2], Malik et al. [3], and Olajuwon et al. [4]. The polymer and textile industries, and plastic manufacturing and food processing are some of the areas where a non-Newtonian fluid is used. Stretchy flow heat transfer is used widely in metal sheet cooling, electronic chips cooling, plastic sheet extrusion in aerodynamic, etc.

A Jeffrey fluid is one of the non-Newtonian fluids that are related to the retardation time and the ratio of relaxation to retardation time. The CCHF model is one of the flow models discussed by Christov [5]. Kasmani et al. [6] concluded that the temperature profile, heat transfer rate, and mass transfer rate rises while magnifying the thermophoresis parameter. The peristalsis flow of a non-constant viscous Jeffrey nanofluid was studied by Alvi et al. [7]. While increasing the Brownian motion and the thermophoresis parameter, the opposite behavior of the concentration profile is identified by Muhammad et al. [8]. Ramly et al. [9] observed that under passive control, the heat and mass transfer rates seem to have opposite behaviors when influenced by the Brownian motion parameter and the thermophoresis parameter.

The effects of non-linear thermal radiation and the Soret and Dufour and stratification effect on an MHD nanofluid flow over a stretchy cylinder was studied by Jagan and Sivasankaran [10]. Li et al. [11] identified that the heat transfer rate rises by magnifying the relaxation time parameter and the mixed convection parameter. The temperature field enhances with a rise in the thermal radiation, and the heat generation parameters

were concluded by Niranjana et al. [12]. Das et al. [13] identified that the fluid temperature of a Jeffrey fluid is higher when compared with a Newtonian fluid. The effects of radiation, chemical reaction, and slip on a magnetoconvection stagnation-point flow in a porous medium were analyzed by Niranjana et al. [14]. Ali et al. [15] observed that the non-linear thermal radiation parameters regulate the momentum and thermal boundary layers. Thermally stratified stretchy flow with CCHF is studied by Hayat et al. [16]. Ferdows et al. [17] examined about the free convective flow in an inclined porous surface. Ramzan et al. [18] investigated the MHD stagnation-point flow of a Williamson fluid with CCHF, homogeneous–heterogeneous reactions, and a convective boundary condition.

Hayat et al. [19] studied three-dimensional incompressible elasto-viscous fluid flow towards a stretchy surface. Unsteady 3D boundary layer flow due to a permeable shrinky sheet was analyzed by Bachok et al. [20]. Shehzad et al. [21] investigated 3D Jeffrey fluid flow over a stretched surface that exhibits a convective boundary condition. A Three-dimensional thermally radiated Jeffrey fluid flow towards a stretchy surface with variable thermal conductivity was examined by Hayat et al. [22]. Raju et al. [23] concluded that heat and mass transfer rate for a flow over a stretchy surface is high. Three-dimensional flow and heat transfer to a Burger’s fluid using the CCHF model was analyzed by Khan et al. [24]. Ramzan et al. [25] examined the supremacy of homogeneous–heterogeneous reactions on the MHD 3D flow of increasing the Maxwell fluid with the CCHF model and convective boundary condition. Hayat et al. [26] identified that Fourier and Cattaneo–Christov heat conduction models remain numerically similar when influenced by an embedding parameter. The three-dimensional Jeffrey fluid boundary layer flow induced by a bi-directional stretchy surface with CCHF model is studied by Hayat et al. [27]. More related study are found in [28–30].

In this paper, an analysis is made on a 3D non-linearly thermally radiated flow of a Jeffrey nanofluid with the CCHF model in the presence of a convective boundary condition towards a bidirectional stretchy surface. The current model with non-linear thermal radiation and convective boundary layer flow is not analyzed by any author, which shows the novelty of the current study. No such investigation is available in the literature, and therefore, the results obtained are novel. The results may be useful to fields such as paper production and plastic sheet production.

2. Mathematical Formulation

Regarding three-dimensional, steady, and incompressible non-linearly thermally radiated Jeffrey nanofluid flow towards a bidirectional stretchy surface CCHF model, the convective boundary condition is considered. The velocity of the stretchy surface along the x -axis and y -axis is assumed as $v_{1,w} = b_1x$ and $v_{2,w} = b_2y$, where b_1 and b_2 are positive constants, as shown in Figure 1. Fluid flow is considered along the z -axis. The governing boundary layer equations for the present analysis (refer to Hayat et al. [27]) can be written as

Continuity Equation

$$\frac{\partial v_1}{\partial x} + \frac{\partial v_2}{\partial y} + \frac{\partial v_3}{\partial z} = 0, \quad (1)$$

Momentum Equation

$$\begin{aligned} v_1 \frac{\partial v_1}{\partial x} + v_2 \frac{\partial v_1}{\partial y} + v_3 \frac{\partial v_1}{\partial z} &= \frac{\nu}{1 + \lambda_1} \frac{\partial^2 v_1}{\partial z^2} + \frac{\nu \lambda_2}{1 + \lambda_1} \left(v_1 \frac{\partial^3 v_1}{\partial x \partial z^2} + v_2 \frac{\partial^3 v_1}{\partial y \partial z^2} \right. \\ &\left. + v_3 \frac{\partial^3 v_1}{\partial z^3} \right) + \frac{\nu \lambda_2}{1 + \lambda_1} \left(\frac{\partial v_1}{\partial z} \frac{\partial^2 v_1}{\partial x \partial z} + \frac{\partial v_2}{\partial z} \frac{\partial^2 v_1}{\partial y \partial z} + \frac{\partial v_3}{\partial z} \frac{\partial^2 v_1}{\partial z^2} \right), \end{aligned} \quad (2)$$

$$v_1 \frac{\partial v_2}{\partial x} + v_2 \frac{\partial v_2}{\partial y} + v_3 \frac{\partial v_2}{\partial z} = \frac{\nu}{1 + \lambda_1} \frac{\partial^2 v_2}{\partial z^2} + \frac{\nu \lambda_2}{1 + \lambda_1} \left(v_1 \frac{\partial^3 v_2}{\partial x \partial z^2} + v_2 \frac{\partial^3 v_2}{\partial y \partial z^2} + v_3 \frac{\partial^3 v_2}{\partial z^3} \right) + \frac{\nu \lambda_2}{1 + \lambda_1} \left(\frac{\partial v_1}{\partial z} \frac{\partial^2 v_2}{\partial x \partial z} + \frac{\partial v_2}{\partial z} \frac{\partial^2 v_2}{\partial y \partial z} + \frac{\partial v_3}{\partial z} \frac{\partial^2 v_2}{\partial z^2} \right), \tag{3}$$

Temperature Equation

$$v_1 \frac{\partial(Te)}{\partial x} + v_2 \frac{\partial(Te)}{\partial y} + v_3 \frac{\partial(Te)}{\partial z} + \lambda_3 \left(v_1^2 \frac{\partial^2(Te)}{\partial x^2} + v_2^2 \frac{\partial^2(Te)}{\partial y^2} + v_3^2 \frac{\partial^2(Te)}{\partial z^2} \right) + \lambda_3 \left(2v_1 v_2 \frac{\partial^2(Te)}{\partial x \partial y} + 2v_1 v_3 \frac{\partial^2(Te)}{\partial x \partial z} + 2v_2 v_3 \frac{\partial^2(Te)}{\partial y \partial z} + \left(v_1 \frac{\partial v_1}{\partial x} + v_2 \frac{\partial v_1}{\partial y} + v_3 \frac{\partial v_1}{\partial z} \right) \frac{\partial(Te)}{\partial x} \right) + \lambda_3 \left(\left(v_1 \frac{\partial v_2}{\partial x} + v_2 \frac{\partial v_2}{\partial y} + v_3 \frac{\partial v_2}{\partial z} \right) \frac{\partial(Te)}{\partial y} + \left(v_1 \frac{\partial v_3}{\partial x} + v_2 \frac{\partial v_3}{\partial y} + v_3 \frac{\partial v_3}{\partial z} \right) \frac{\partial(Te)}{\partial z} \right) = \frac{k}{(\rho c_p)} \left(\frac{\partial^2(Te)}{\partial z^2} \right) + \tau D_B \left(\frac{\partial(Te)}{\partial z} \frac{\partial(Cn)}{\partial z} \right) + \frac{\tau D_{Te}}{Te_\infty} \left(\frac{\partial(Te)}{\partial z} \right)^2 + \frac{1}{(\rho c_p)} \frac{16 \sigma^* Te^3}{3 k^*} \frac{\partial^2(Te)}{\partial z^2}, \tag{4}$$

Nano-Particle Volume Fraction Equation

$$v_1 \frac{\partial(Cn)}{\partial x} + v_2 \frac{\partial(Cn)}{\partial y} + v_3 \frac{\partial(Cn)}{\partial z} = D_B \left(\frac{\partial^2(Cn)}{\partial z^2} \right) + \frac{D_{Te}}{Te_\infty} \left(\frac{\partial^2(Te)}{\partial z^2} \right), \tag{5}$$

where the boundary conditions (refer to Hayat et al. [27] and Shehzad et al. [21]) are

$$v_1 = v_{1,w} = b_1 x, v_2 = v_{2,w} = b_2 y, v_3 = 0, \\ -k \frac{\partial(Te)}{\partial z} = h(Te_f - Te), Cn = Cn_f \text{ at } z = 0. \\ v_1 \rightarrow 0, v_2 \rightarrow 0, Te \rightarrow Te_\infty, Cn \rightarrow Cn_\infty \text{ as } z \rightarrow \infty. \tag{6}$$

The transformations (refer to Hayat et al. [27]) are

$$\zeta = z \sqrt{\frac{b_1}{\nu}}, v_1 = b_1 x \phi_1'(\zeta), v_2 = b_1 y \phi_2'(\zeta), v_3 = -\sqrt{b_1 \nu} (\phi_1(\zeta) + \phi_2(\zeta)), \\ \phi_3(\zeta) = \frac{Te - Te_\infty}{Te_f - Te_\infty}, \phi_4(\zeta) = \frac{Cn - Cn_\infty}{Cn_f - Cn_\infty}. \tag{7}$$

Equation (1) satisfies identically, and Equations (2)–(6) are reduced to Equations (8)–(12) using Equation (7).

$$\phi_1''' + (1 + \lambda_1) [\phi_1''(\phi_1 + \phi_2) - \phi_1'^2] + \beta [\phi_1''^2 - (\phi_1 + \phi_2)\phi_1^{iv} - \phi_1'''\phi_2'] = 0, \quad (8)$$

$$\phi_2''' + (1 + \lambda_1) [(\phi_1 + \phi_2)\phi_2'' - \phi_2'^2] + \beta [\phi_2''^2 - (\phi_1 + \phi_2)\phi_2^{iv} - \phi_2'''\phi_1'] = 0, \quad (9)$$

$$\begin{aligned} & \left(1 + \frac{4}{3}Rd\right)\phi_3'' + \frac{4}{3}Rd [(\theta_w - 1)^3 (3\phi_3^2(\phi_3')^2 + \phi_3^3\phi_3'')] \\ & + 3(\theta_w - 1)^2 (2\phi_3(\phi_3')^2 + \phi_3^2\phi_3'') + 4Rd [(\theta_w - 1)((\phi_3')^2 + \phi_3\phi_3'')] \\ & + Pr(\phi_1 + \phi_2)\phi_3' - \gamma Pr [(\phi_1 + \phi_2)^2\phi_3'' + \phi_3'(\phi_1 + \phi_2)(\phi_1' + \phi_2')] \\ & + PrNt(\phi_3')^2 + PrNb\phi_3'\phi_4' = 0, \end{aligned} \quad (10)$$

$$\phi_4'' + Sc(\phi_1 + \phi_2)\phi_4' + \frac{Nt}{Nb}\phi_3'' = 0, \quad (11)$$

$$\begin{aligned} \phi_1(0) = 0, \phi_2(0) = 0, \phi_1'(0) = 1, \phi_2'(0) = c, \phi_3'(0) = -\alpha(1 - \phi_3(0)), \\ \phi_4(0) = 1 \end{aligned} \quad (12)$$

$$\phi_1'(\zeta) \rightarrow 0, \phi_2'(\zeta) \rightarrow 0, \phi_3(\zeta) \rightarrow 0, \phi_4(\zeta) \rightarrow 0 \text{ as } \zeta \rightarrow \infty.$$

where

$$\begin{aligned} \alpha &= \frac{h\sqrt{\nu/b_1}}{k}, \beta = \lambda_2 b_1, c = \frac{b_2}{b_1}, \gamma = \lambda_3 b_1, Nb = \frac{\tau D_B (Cn_f - Cn_\infty)}{\nu}, \\ Nt &= \frac{\tau D_{Te} (Te_f - Te_\infty)}{\nu Te_\infty}, Pr = \frac{\mu c_p}{k}, Rd = \frac{4\sigma^* Te_\infty^3}{kk^*}, Sc = \frac{\nu}{D}, \\ \theta_w &= \frac{Te_f}{Te_\infty}. \end{aligned} \quad (13)$$

The skin-friction coefficient, and the local Nusselt and Sherwood number are given by

$$Re_x^{1/2} C_{f_x} = \left(\frac{2}{1 + \lambda_1}\right) \phi_1''(0), \quad (14)$$

$$Re_y^{1/2} C_{f_y} = \left(\frac{2}{1 + \lambda_1}\right) \phi_2''(0), \quad (15)$$

$$Re_x^{-1/2} Nu = -\left(1 + \frac{4}{3}Rd(\theta_w)^3\right) \phi_3'(0), \quad (16)$$

$$Re_x^{-1/2} Sh = -\phi_4'(0). \quad (17)$$

where $Re_x = \frac{v_{1,w}x}{\nu}$ and $Re_y = \frac{v_{2,w}y}{\nu}$ are Reynolds numbers.

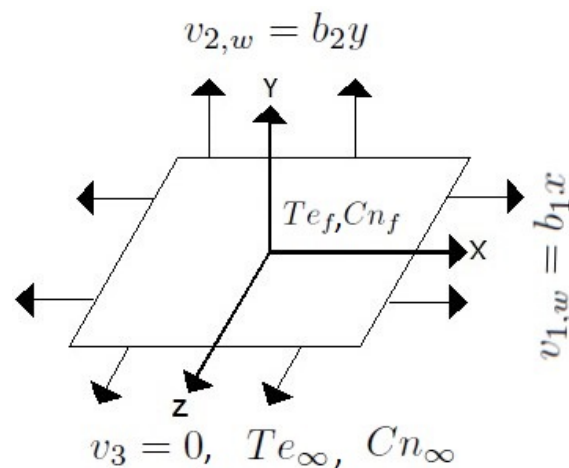


Figure 1. Physical diagram.

3. Convergence of the Solution

Equations (8)–(11), subject to Equation (12), are solved using HAM by choosing the initial boundary approximations, auxiliary function, and auxiliary linear operators (refer to Hayat et al. [27]) as

$$\begin{aligned} \phi_{1,0}(\zeta) &= 1 - \exp(-\zeta), \quad \phi_{2,0}(\zeta) = c(1 - \exp(-\zeta)), \\ \phi_{3,0}(\zeta) &= \frac{\alpha}{1 + \alpha} \exp(-\zeta), \quad \phi_{4,0}(\zeta) = \exp(-\zeta). \end{aligned} \tag{18}$$

$$H(\zeta) = 1. \tag{19}$$

$$\begin{aligned} L_{\phi_1}(\phi_1) &= \frac{d^3\phi_1}{d\zeta^3} - \frac{d\phi_1}{d\zeta}, \quad L_{\phi_2}(\phi_2) = \frac{d^3\phi_2}{d\zeta^3} - \frac{d\phi_2}{d\zeta}, \\ L_{\phi_3}(\phi_3) &= \frac{d^2\phi_3}{d\zeta^2} - \phi_3, \quad L_{\phi_4}(\phi_4) = \frac{d^2\phi_4}{d\zeta^2} - \phi_4. \end{aligned} \tag{20}$$

which satisfies the property

$$L_{\phi_1}[A_1 + A_2 \exp(-\zeta) + A_3 \exp(\zeta)] = 0, \tag{21}$$

$$L_{\phi_2}[A_4 + A_5 \exp(-\zeta) + A_6 \exp(\zeta)] = 0, \tag{22}$$

$$L_{\phi_3}[A_7 \exp(-\zeta) + A_8 \exp(\zeta)] = 0, \tag{23}$$

$$L_{\phi_4}[A_9 \exp(-\zeta) + A_{10} \exp(\zeta)] = 0. \tag{24}$$

where A_1 to A_{10} are arbitrary constants. Mathematica software is used to solve the above HAM equations. The equations obtained contain the parameters $h_{\theta_1}, h_{\phi_1}, h_{\phi_2}$, and h_s . The h -curve is plotted for $\alpha = 0.3, \beta = 0.2, c = 0.3, \gamma = 0.2, \lambda_1 = 0.3, Nb = 0.2, Nt = 0.2, Pr = 1.0, Rd = 0.3, Sc = 0.6$, and $\theta_w = 0.3$. From Figure 2, it is clear that the range for the admissible values of $h_{\phi_1}, h_{\phi_2}, h_{\phi_3}$, and h_{ϕ_4} are $-1.5 \leq h_{\phi_1} \leq -0.2, -1.4 \leq h_{\phi_2} \leq -0.1, -1.5 \leq h_{\phi_3} \leq -0.1$, and $-1.4 \leq h_{\phi_4} \leq -0.3$ at the 20th-order approximation.

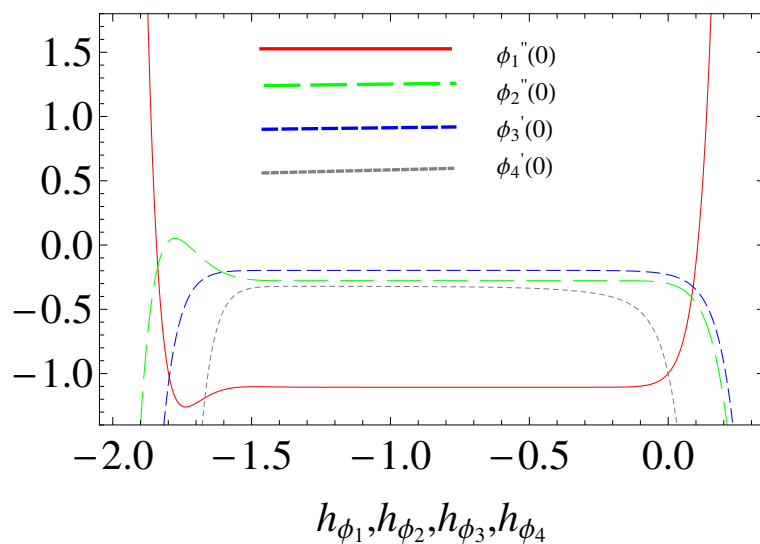


Figure 2. h -curve for $\phi_1''(0), \phi_2''(0), \phi_3'(0)$, and $\phi_4'(0)$.

The convergence value is tabulated in Table 1 for different orders of approximations. In order to vary our results, we made a comparison of the results for $-\phi_1''(0), -\phi_2''(0)$ and $-\phi_3'(0)$ when $\beta = \gamma = 0.2, c = \lambda = 0.3, Pr = 1$, with Hayat et al. [27]. We found a good agreement between the present results and the available results.

Table 1. Convergence of the series $-\phi_1''(0)$, $-\phi_2''(0)$, $-\phi_3'(0)$, and $-\phi_4'(0)$ for $\alpha = 0.3$, $\beta = 0.2$, $c = 0.3$, $\gamma = 0.2$, $\lambda_1 = 0.3$, $Nb = 0.2$, $Nt = 0.2$, $Pr = 1.0$, $Rd = 0.3$, $Sc = 0.6$, and $\theta_w = 0.3$.

<i>m</i> -th-Order Approximation	$-\phi_1''(0)$	$-\phi_2''(0)$	$-\phi_3'(0)$	$-\phi_4'(0)$
1	1.0625	0.2873	0.2186	0.7573
5	1.1055	0.2774	0.2016	0.4537
10	1.1064	0.2774	0.1980	0.3766
15	1.1064	0.2774	0.1974	0.3487
20	1.1064	0.2774	0.1974	0.3357
25	1.1064	0.2774	0.1974	0.3292
30	1.1064	0.2774	0.1975	0.3258
35	1.1064	0.2774	0.1975	0.3239

In Tables 2 and 3, the skin-friction coefficient, and the Nusselt number and Sherwood number are tabulated for various parameters with different sets of values.

Table 2. Numerical values of the skin-friction coefficient for the fixed values $\alpha = 0.3$, $\gamma = 0.2$, $Nb = 0.2$, $Nt = 0.2$, $Pr = 1.0$, $Rd = 0.3$, $Sc = 0.6$, and $\theta_w = 0.3$.

λ_1	β	c	$-Re_x^{1/2}C_{f_x}$	$-Re_y^{1/2}C_{f_y}$
0.1	0.2	0.3	1.8505	0.4639
0.2	0.2	0.3	1.7717	0.4441
0.3	0.2	0.3	1.7022	0.4267
0.4	0.2	0.3	1.6403	0.4112
0.5	0.2	0.3	1.5847	0.3973
0.3	0.1	0.3	1.7739	0.4268
0.3	0.2	0.3	1.7022	0.4267
0.3	0.3	0.3	1.6387	0.4265
0.3	0.4	0.3	1.5819	0.4263
0.3	0.5	0.3	1.5306	0.4259
0.3	0.2	0.1	1.6361	0.1204
0.3	0.2	0.2	1.6696	0.2641
0.3	0.2	0.3	1.7022	0.4267
0.3	0.2	0.4	1.7341	0.6053
0.3	0.2	0.5	1.7656	0.7976

Table 3. Numerical values of the Nusselt number and Sherwood number for the fixed values $\alpha = 0.3$, $c = 0.3$, $Pr = 1.0$, $Sc = 0.6$, and $\theta_w = 0.3$.

Rd	λ_1	β	Nt	Nb	γ	$Re_x^{-1/2}Nu$	$Re_x^{-1/2}Sh$
0.1	0.3	0.2	0.2	0.2	0.2	0.2019	0.3453
0.2	0.3	0.2	0.2	0.2	0.2	0.2007	0.3471
0.3	0.3	0.2	0.2	0.2	0.2	0.1996	0.3487
0.4	0.3	0.2	0.2	0.2	0.2	0.1986	0.3503
0.5	0.3	0.2	0.2	0.2	0.2	0.1976	0.3518
0.3	0.1	0.2	0.2	0.2	0.2	0.2016	0.3613
0.3	0.2	0.2	0.2	0.2	0.2	0.2006	0.3548
0.3	0.3	0.2	0.2	0.2	0.2	0.1996	0.3487
0.3	0.4	0.2	0.2	0.2	0.2	0.1986	0.3431
0.3	0.5	0.2	0.2	0.2	0.2	0.1977	0.3380
0.3	0.3	0.1	0.2	0.2	0.2	0.1985	0.3424
0.3	0.3	0.2	0.2	0.2	0.2	0.1996	0.3487
0.3	0.3	0.3	0.2	0.2	0.2	0.2005	0.3546
0.3	0.3	0.4	0.2	0.2	0.2	0.2014	0.3600
0.3	0.3	0.5	0.2	0.2	0.2	0.2022	0.3651
0.3	0.3	0.2	0.1	0.2	0.2	0.2001	0.4146
0.3	0.3	0.2	0.2	0.2	0.2	0.1996	0.3487
0.3	0.3	0.2	0.3	0.2	0.2	0.1990	0.2835
0.3	0.3	0.2	0.4	0.2	0.2	0.1985	0.2191
0.3	0.3	0.2	0.5	0.2	0.2	0.1979	0.1553
0.3	0.3	0.2	0.2	0.1	0.2	0.2020	0.2098
0.3	0.3	0.2	0.2	0.2	0.2	0.1996	0.3487
0.3	0.3	0.2	0.2	0.3	0.2	0.1971	0.3951
0.3	0.3	0.2	0.2	0.4	0.2	0.1946	0.4183
0.3	0.3	0.2	0.2	0.5	0.2	0.1920	0.4323
0.3	0.3	0.2	0.2	0.2	0.1	0.1985	0.3496
0.3	0.3	0.2	0.2	0.2	0.2	0.1996	0.3487
0.3	0.3	0.2	0.2	0.2	0.3	0.2007	0.3478
0.3	0.3	0.2	0.2	0.2	0.4	0.2019	0.3467
0.3	0.3	0.2	0.2	0.2	0.5	0.2032	0.3456

4. Computational Results and Discussion

The supremacy of embedding the parameters involved in the study are discussed here. The agreement is found to be good while comparing the current study with Hayat et al. [27] for $\beta = 0.2$, $\lambda_1 = 0.3$, and $c = 0.3$ (see Table 4). In Figure 3, the ratio of relaxation to the retardation time (λ_1) is plotted with different values for $\phi_1'(\zeta)$, $\phi_2'(\zeta)$, $\phi_3(\zeta)$, and $\phi_4(\zeta)$. It is clear that $\phi_1'(\zeta)$ and $\phi_2'(\zeta)$ rise while boosting (λ_1), whereas $\phi_3(\zeta)$ and $\phi_4(\zeta)$ diminish. In Figure 4, it is found that when the Deborah number (β) is raised, $\phi_1'(\zeta)$ and $\phi_2'(\zeta)$ enhance, and at the same time, the temperature and concentration profile diminishes because the retardation will be raised while raising β .

Table 4. Comparison of current study with Hayat et al. [27] for $\beta = 0.2$, $\lambda_1 = 0.3$, and $c = 0.3$.

<i>m</i> -th-Order Approximation	Hayat et al. [27] $-\phi_1''(0)$	Present $-\phi_1''(0)$	Hayat et al. [27] $-\phi_2''(0)$	Present $-\phi_2''(0)$
1	1.10000	1.0375	0.27960	0.29235
5	1.10638	1.0947	0.27744	0.27983
10	1.10643	1.1053	0.27737	0.27753
15	1.10643	1.10633	0.27737	0.27737
20	1.10643	1.10643	0.27737	0.27737
25	1.10643	1.10643	0.27737	0.27737
35	1.10643	1.10643	0.27737	0.27737
50	1.10643	1.10643	0.27737	0.27737

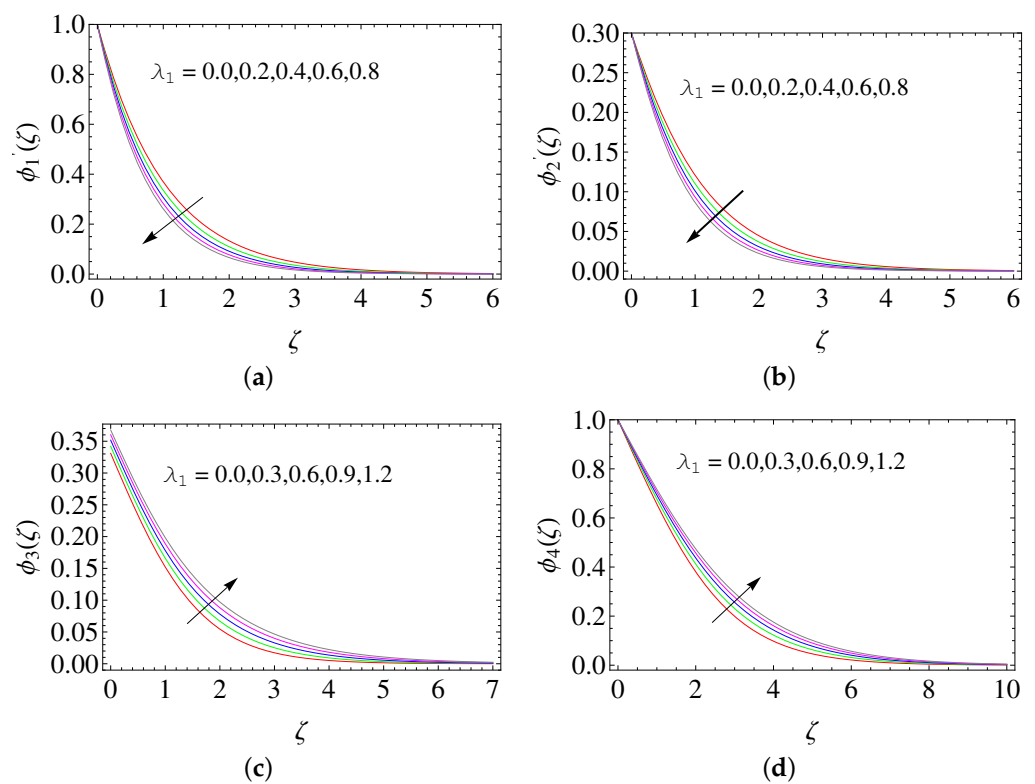


Figure 3. Influence of λ_1 on (a) $\phi_1'(\zeta)$, (b) $\phi_2'(\zeta)$, (c) $\phi_3(\zeta)$, and (d) $\phi_4(\zeta)$.

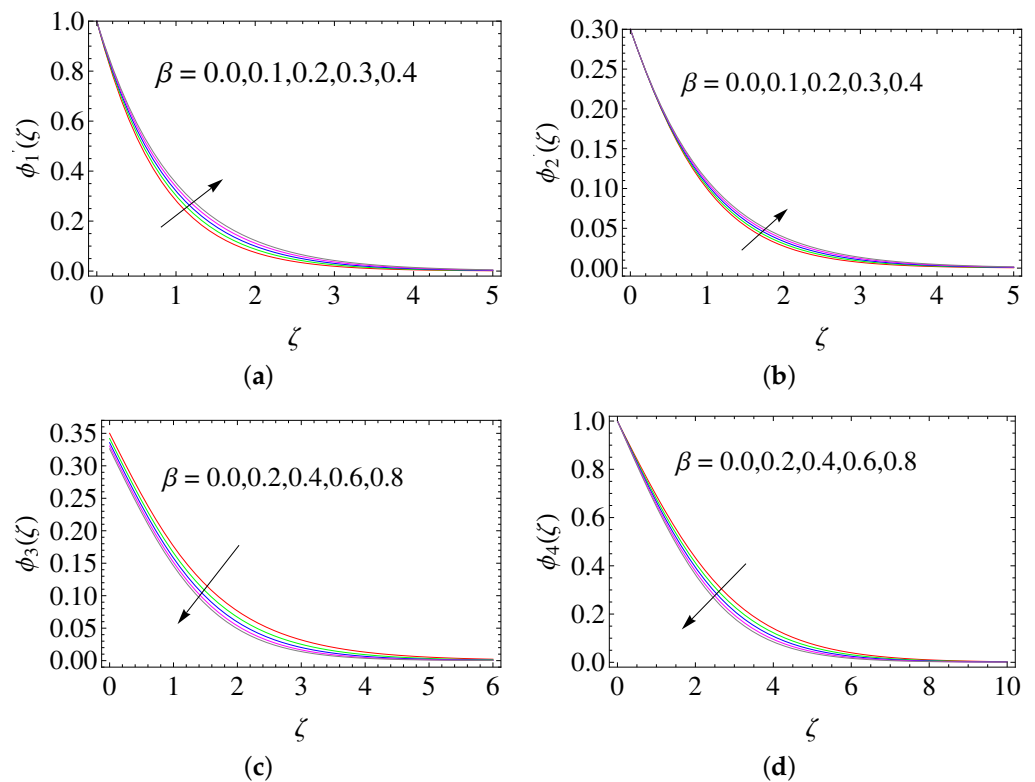


Figure 4. Influence of β on (a) $\phi_1'(\zeta)$, (b) $\phi_2'(\zeta)$, (c) $\phi_3(\zeta)$, and (d) $\phi_4(\zeta)$.

The supremacy of the ratio of stretching rates (c) on $\phi_2'(\zeta)$, $\phi_3(\zeta)$, and $\phi_4(\zeta)$ is analyzed in Figure 5. It is noticed that $\phi_2'(\zeta)$ enlarges while boosting c , whereas $\phi_3(\zeta)$ and $\phi_4(\zeta)$ diminish. Magnifying the radiation parameter leads to the generation of more heat energy to flow, which leads to a rise in the temperature profile (see Figure 6a). From Figure 6b, it is clear that the temperature profile declines by magnifying the thermal relaxation time parameter (γ). The concentration profile magnifies with a rise in the thermal Biot number (α) (see Figure 6c).

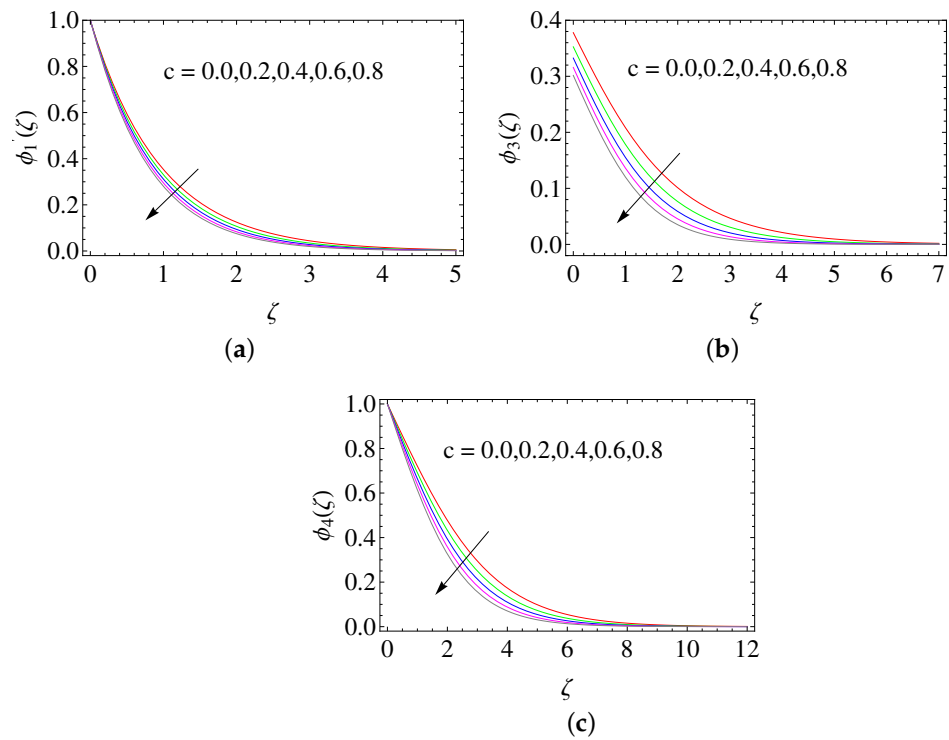


Figure 5. Influence of c on (a) $\phi_1'(\zeta)$, (b) $\phi_3(\zeta)$, and (c) $\phi_4(\zeta)$.

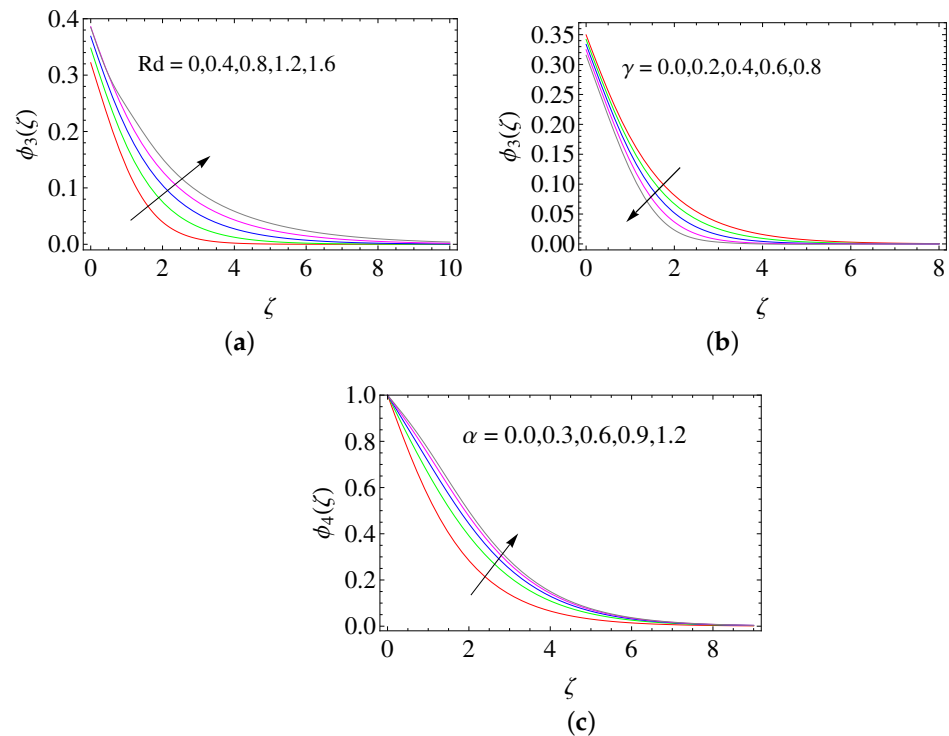


Figure 6. Influence of (a) Rd and (b) γ on $\phi_3(\zeta)$, and (c) α on $\phi_4(\zeta)$.

The skin-friction coefficient along the x- and y-directions rises upon boosting the ratio of the relaxation to retardation time (λ_1) (see Figure 7). From Figure 8, it is clear that the local Nusselt number diminishes by magnifying both Rd . Also, the local Nusselt number enhances by raising α . In Figure 9, the local Nusselt number diminishes on raising λ_1 and Nb . From Figure 10, it is observed that local Sherwood number enhances with a rise in Rd and Nb .

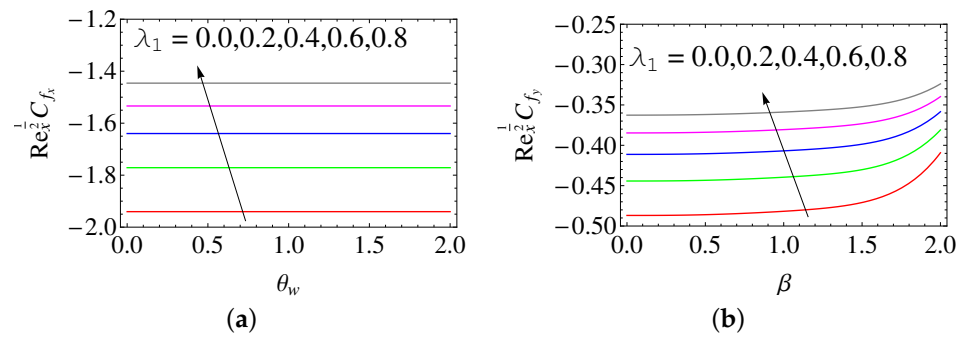


Figure 7. Influence of λ_1 on (a) $Re_x^{-1/2} C_{f_x}$ and (b) $Re_y^{-1/2} C_{f_y}$.

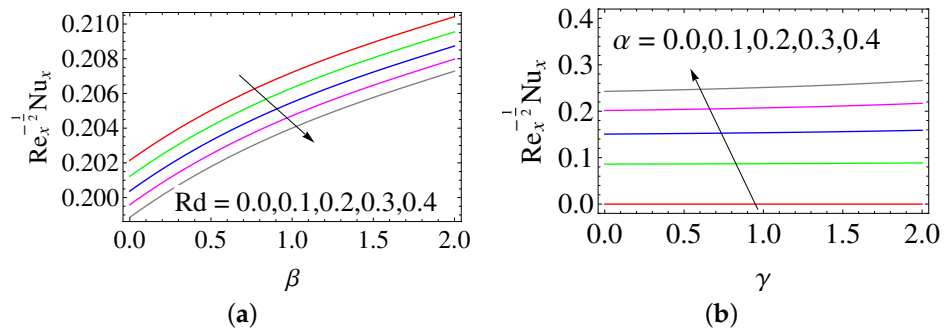


Figure 8. Influence of (a) Rd and (b) α on $Re_x^{-1/2} Nu_x$.

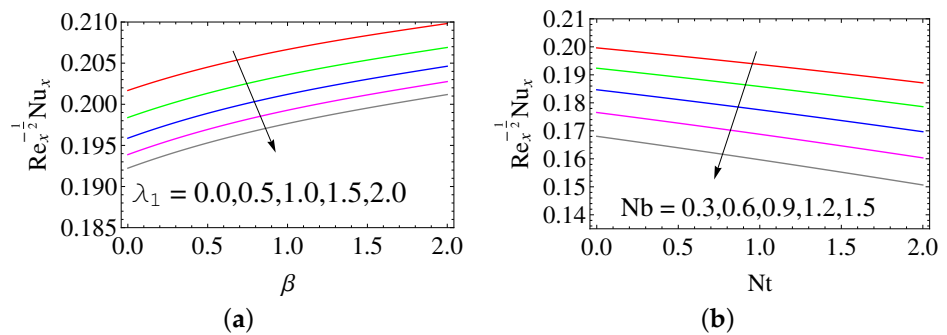


Figure 9. Influence of (a) λ_1 and (b) Nb on $Re_x^{-1/2} Nu_x$.

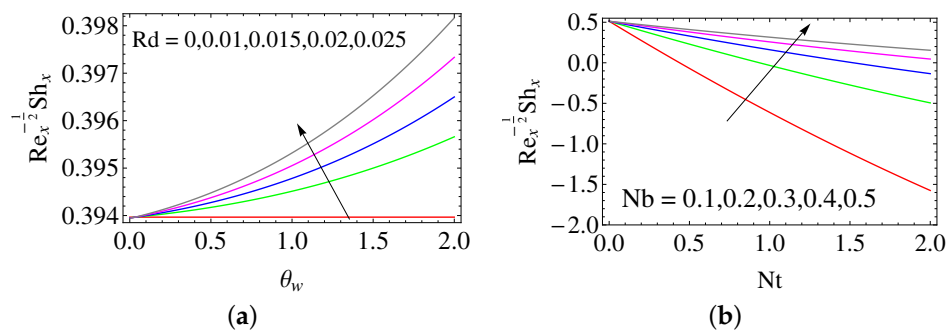


Figure 10. Influence of (a) Rd and (b) Nb on $Re_x^{-1/2} Sh_x$.

The regression equation for skin friction with a variation in the ratio of relaxation to retardation time (λ_1), Deborah number (β), and the ratio of stretching rates (c) are

$$Re_x^{1/2} C_{f_x} = -1.9288 + 0.6631 * \lambda_1 + 0.6057 * \beta - 0.3236 * c. \tag{25}$$

$$Re_y^{1/2} C_{f_y} = 0.0203 + 0.1662 * \lambda_1 + 0.0249 * \beta - 1.6956 * c. \tag{26}$$

The regression equation for the Nusselt number and the Sherwood number with variations in the radiation parameter (Rd), Deborah number (β), thermophoresis parameter (Nt), Brownian motion parameter (Nb), and thermal relaxation time parameter (γ) are

$$Re_x^{1/2}Nu = 0.2077 - 0.0106 * Rd - 0.0097 * \lambda_1 + 0.0088 * \beta - 0.0056 * Nt - 0.0252 * Nb + 0.0117 * \gamma. \quad (27)$$

$$Re_x^{1/2}Sh = 0.3847 + 0.0161 * Rd - 0.0583 * \lambda_1 + 0.0742 * \beta - 0.6286 * Nt + 0.4019 * Nb + 0.0083 * \gamma. \quad (28)$$

5. Conclusions

The study of the 3D non-linearly thermally radiated flow of a Jeffrey nanofluid with the CCHF model in the presence of a convective boundary condition is presented. The following are the outcomes of this analysis:

- The thickening of the thermal boundary occurs while raising the thermal radiation.
- On increasing the thermal radiation, the local heat transfer diminishes and the local heat transfer raises with a raise in the Deborah number.
- The thickness of the momentum boundary layer reduces by boosting the ratio of the relaxation to retardation time; however, the skin friction rises by raising the ratio of the relaxation to retardation time.
- While boosting the thermal Biot number, the thermal boundary layer thickness rises, which results in a rise in the heat transfer rate.
- The local heat (mass) transfer rate diminishes (rises) when the Brownian motion parameter is raised.

Author Contributions: Conceptualization, K.J. and S.S.; methodology, K.J. and S.S.; software, K.J.; validation, K.J.; formal analysis, K.J. and S.S.; investigation, K.J. and S.S.; resources, K.J. and S.S.; writing—original draft preparation, K.J. and S.S.; writing—review and editing, K.J. and S.S.; visualization, K.J.; supervision, S.S. All authors have read and agreed to the published version of the manuscript.

Funding: This research received no external funding.

Conflicts of Interest: The authors declare no conflict of interest.

Abbreviations

The following abbreviations are used in this manuscript:

CCHF	Cattaneo–Christov heat flux
HAM	Homotopy Analysis Method

Nomenclature

c	ratio of stretching rates
c_p	specific heat
h	heat transfer coefficient
k	thermal conductivity
k^*	mean absorption coefficient
v_1, v_2, v_3	velocity components taken along the x-, y- and z-axes
Cn	concentration
D_B	Brownian motion
D_T	thermophoresis coefficient
Nb	Brownian motion parameter
Nt	thermophoresis parameter
Pr	Prandtl number
q	heat flux
Rd	radiation parameter
Sc	Schmidt number
Te	temperature

Greek Symbols

α	thermal Biot number
β	Deborah number
γ	thermal relaxation time parameter
λ_1	ratio of relaxation to retardation time
λ_2	retardation time
λ_3	thermal relaxation
ν	kinematic viscosity
ρ	density
σ^*	Stefan–Boltzmann constant
τ	ratio between the effective nanoparticle materials and fluid heat capacity
θ_w	temperature ratio parameter

References

- Halim, N.A.; Sivasankaran, S.; Noor, N.F.M. Active and passive controls of the Williamson stagnation nanofluid flow over a stretching/shrinking surface. *Neural Comput. Appl.* **2016**, *28*, 1023–1033. [[CrossRef](#)]
- Mahanthesh, B.; Gireesha, B.J.; Thammaanna, G.T.; Shehzad, S.A.; Abbasi, F.M.; Gorla, R.S.R. Nonlinear convection in nano Maxwell fluid with nonlinear thermal radiation: A three-dimensional study. *Alex. Eng. J.* **2018**, *57*, 1927–1935. [[CrossRef](#)]
- Malik, M.Y.; Khan, M.; Salahuddin, T.; Khan, I. Variable viscosity and MHD flow in Casson fluid with Cattaneo–Christov heat flux model: Using Keller box method. *Eng. Sci. Technol. Int.* **2016**, *19*, 1985–1992. [[CrossRef](#)]
- Olajuwon, B.I.; Oahimire, J.I.; Ferdow, M. Effect of thermal radiation and Hall current on heat and mass transfer of unsteady MHD flow of a viscoelastic micropolar fluid through a porous medium. *Eng. Sci. Technol. Int.* **2014**, *17*, 185–193. [[CrossRef](#)]
- Christov, C.I. On frame indifferent formulation of the Maxwell–Cattaneo model of finite-speed heat conduction. *Mech. Res. Commun.* **2009**, *36*, 481–486. [[CrossRef](#)]
- Kasmani, R.M.; Sivasankaran, S.; Bhuvanewari, M.; Siri, Z. Effect of Chemical Reaction on Convective Heat Transfer of Boundary Layer Flow in Nanofluid over a Wedge with Heat Generation/Absorption and Suction. *J. Appl. Fluid Mech.* **2016**, *9*, 379–388. [[CrossRef](#)]
- Alvi, N.; Latif, T.; Hussain, Q.; Asghar, S. Peristalsis of nonconstant viscosity Jeffrey fluid with nanoparticles. *Results Phys.* **2016**, *6*, 1109–1125. [[CrossRef](#)]
- Muhammad, N.; Nadeem, S.; Mustafa, T. Squeezed flow of a nanofluid with Cattaneo–Christov heat and mass fluxes. *Results Phys.* **2017**, *7*, 862–869. [[CrossRef](#)]
- Ramly, N.A.; Sivasankaran, S.; Noor, N.F.M. Numerical solution of Cheng–Minkowycz natural convection nanofluid flow with zero flux. *AIP Conf. Proc.* **2016**, *1750*, 030020.
- Jagan, K.; Sivasankaran, S. Soret & Dufour and triple stratification effect on MHD flow with velocity slip towards a stretching cylinder. *Math. Comput. Appl.* **2022**, *27*, 25.
- Li, J.; Zheng, L.; Liu, L. MHD viscoelastic flow and heat transfer over a vertical stretching sheet with Cattaneo–Christov heat flux effects. *J. Mol. Liq.* **2016**, *221*, 19–25. [[CrossRef](#)]
- Niranjana, H.; Sivasankaran, S.; Bhuvanewari, M.; Siri, Z. Effects of chemical reaction on MHD mixed convection stagnation point flow toward a vertical plate in a porous medium with radiation and heat generation. *J. Phys. Conf.* **2015**, *662*, 012014.
- Das, K.; Acharya, N.; Kundu, P.K. Radiative flow of MHD Jeffrey fluid past a stretching sheet with surface slip and melting heat transfer. *Alex. Eng. J.* **2015**, *54*, 815–821. [[CrossRef](#)]
- Niranjana, H.; Sivasankaran, S.; Bhuvanewari, M. Analytical and Numerical Study on Magnetoconvection Stagnation-Point Flow in a Porous Medium with Chemical Reaction, Radiation, and Slip Effects. *Math. Probl. Eng.* **2016**, *2016*, 4017076. [[CrossRef](#)]
- Ali, M.E.; Sandeep, N. Cattaneo–Christov model for radiative heat transfer of magnetohydrodynamic Casson-ferrofluid: A numerical study. *Results Phys.* **2017**, *7*, 21–30. [[CrossRef](#)]
- Hayat, T.; Khan, M.I.; Farooq, M.; Alsaedi, A.; Khan, M.I. Thermally stratified stretching flow with Cattaneo–Christov heat flux. *Int. J. Heat Mass Transf.* **2017**, *106*, 289–294. [[CrossRef](#)]
- Ferdows, M.; Kaino, K.; Sivasankaran, S. Free convective flow in an inclined porous surface. *J. Porous Media* **2019**, *12*, 997–1003.
- Ramzan, M.; Bilal, M.; Chung, J.D. MHD stagnation point Cattaneo–Christov heat flux in Williamson fluid flow with homogeneous-heterogeneous reactions and convective boundary condition. *J. Mol. Liq.* **2017**, *225*, 856–862. [[CrossRef](#)]
- Hayat, T.; Sajid, M.; Pop, I. Three-dimensional flow over a stretching surface in a viscoelastic fluid. *Nonlinear Anal. Real World Appl.* **2008**, *9*, 1811–1822. [[CrossRef](#)]
- Bachok, N.; Ishak, A.; Pop, I. Unsteady three-dimensional boundary layer flow due to a permeable shrinking sheet. *Appl. Math. Mech.* **2010**, *31*, 1421–1428. [[CrossRef](#)]
- Shehzad, S.A.; Alsaedi, A.; Hayat, T. Three-dimensional flow of Jeffrey fluid with convective surface boundary conditions. *Int. J. Heat Mass Transf.* **2012**, *55*, 3971–3976. [[CrossRef](#)]
- Hayat, T.; Shehzad, S.A.; Alsaedi, A. Three-dimensional stretched flow of Jeffrey fluid with variable thermal conductivity and thermal radiation. *Appl. Math. Mech.* **2013**, *34*, 823–832. [[CrossRef](#)]

23. Raju, C.S.K.; Sandeep, N.; Gnaneswara Reddy, M. Effect of Nonlinear Thermal Radiation on 3D Jeffrey Fluid Flow in the Presence of Homogeneous–Heterogeneous Reactions. *Int. J. Eng. Res.* **2015**, *21*, 52–68. [[CrossRef](#)]
24. Khan, M.; Khan, W.A. Three-dimensional flow and heat transfer to burgers fluid using Cattaneo-Christov heat flux model. *J. Mol. Liq.* **2016**, *221*, 651–657. [[CrossRef](#)]
25. Ramzan, M.; Bilal, M.; Chung, J.D. Influence of homogeneous-heterogeneous reactions on MHD 3D Maxwell fluid flow with Cattaneo-Christov heat flux and convective boundary condition. *J. Mol. Liq.* **2017**, *230*, 415–422. [[CrossRef](#)]
26. Hayat, T.; Qayyum, S.; Imtiaz, M.; Alsaedi, A. Three-dimensional rotating flow of Jeffrey fluid for Cattaneo-Christov heat flux model. *AIP Adv.* **2016**, *6*, 025012. [[CrossRef](#)]
27. Hayat, T.; Muhammad, T.; Mustafa, M.; Alsaedi, A. Three-dimensional flow of Jeffrey fluid with Cattaneo-Christov heat flux: An application to non-Fourier heat flux theory. *Chin. J. Phys.* **2017**, *55*, 1067–1077. [[CrossRef](#)]
28. Bagh, A.; Thirupathi, T.; Danial, H.; Nadeem, S.; Saleem, R. Finite element analysis on transient MHD 3D rotating flow of Maxwell and tangent hyperbolic nanofluid past a bidirectional stretching sheet with Cattaneo Christov heat flux model. *Therm. Sci. Eng. Prog.* **2022**, *28*, 101089.
29. Bagh, A.; Imran, S.; Ali, A.; Norazak, S.; Liaqat, A.; Amir, H. Significance of Lorentz and Coriolis forces on dynamics of water based silver tiny particles via finite element simulation. *Ain Shams Eng. J.* **2022**, *13*, 101572.
30. Bagh, A.; Anum, S.; Imran, S.; Qasem, A.; Fahd, J. Significance of suction/injection, gravity modulation, thermal radiation, and magnetohydrodynamic on dynamics of micropolar fluid subject to an inclined sheet via finite element approach. *Case Stud. Therm. Eng.* **2021**, *28*, 101537.